Dam Deformation Monitoring using Cloud-Based P-SBAS Algorithm: The Kramis Dam Case (Algeria)

Kamel Hasni
Space Geodesy Department, Centre of Space Techniques (CTS), Algeria
khasni@cts.asal.dz (corresponding author)

Bachir Gourine
National High School of Geodetic Sciences and Space Techniques (ENSGTS), Algeria
bachirgourine@yahoo.com

Mohammed El Amin Larabi
Earth Observation Department, Centre of Space Techniques (CTS), Algeria
arabi.mohamed.lamine@gmail.com

Received: 17 March 2023 | Revised: 6 April 2023 | Accepted: 12 April 2023

 DOI: https://doi.org/10.48084/etasr.5857

ABSTRACT

This paper presents the application of the Parallel Small Baseline Subset (P-SBAS) algorithm, provided by the Geohazards Exploitation Platform for the precise monitoring of an earth dam's ground deformation using C-band Sentinel-1 data. The test site object of this study was the Kramis dam, located in the Mostaganem State, Western Algeria. Among the multiple advanced DInSAR techniques, SBAS is very adequate for long-term displacement monitoring in areas with changing terrain and vegetation. Ten corner reflectors were installed as a backscattered radar signal amplification tool to reduce the effect of temporal decorrelation and delineate the dam area. Four Sentinel-1 A and B satellite tracks were available (T30, T37, T103, and T110) to measure displacements, in the Line of Site (LoS) direction, for two years since the installation of the CRs in July 2019. The results showed a subsiding area on the left bank of the dam dike, with a velocity of 4mm/yr, and an uplifting rate of 3-4mm/yr in the upper part of the dike. The entire 3-dimensional vector of displacement of the dam vicinity was estimated using the least-squares method, proving a better understanding of the dam's temporal deformation, particularly for dams with a high exposure factor and associated risk.

Keywords-dam deformation; Kramis; P-SBAS; time series

I. INTRODUCTION

In Algeria, embankment dams are the backbone of the water management infrastructure [1]. Despite their advantages in terms of strength and structure, these structures must be equipped with a precise monitoring system to ensure their safety and guarantee their durability [2-3]. Monitoring surface displacements is a tool to control risk phenomena, in particular, the overall instabilities within the natural embankments of the dike and the reservoir [4-6]. The primary purpose of monitoring and auscultation is to survey the behavior of the dam over time, maintain its operation, and ensure the safety of the structure to withstand the agglomerations downstream of the dam [7]. Two aspects of precise surveillance, commonly known by the name of auscultation, arise. The first is internal auscultation, where dam monitoring is performed on a regular basis with different types of instruments, such as piezometers, total stress cells, settlement devices, or triaxial deformation tubes. The second type of auscultation is external. This process aims to precisely measure the displacements and superficial deformations incurred using geodetic and topographic techniques. In addition to the Global Navigation Satellite System (GNSS), Interferometric Synthetic Aperture Radar (InSAR) methods have been proposed as reliable and precise tools for the apprehension of dam deformations [8-10].

Investigations and observations conducted during field surveys are time-consuming, expensive, and have low reproducibility. In contrast, Multi-Temporal InSAR (MT-InSAR) can retrieve historical displacements, identify minute ground anomalies, fully reveal the geographic distributions of surface deformations, and identify displacement boundaries with a high spatial resolution of meters and an accuracy of centimeters to millimeters [11]. Today, MT-InSAR methods, such as PSInSAR, SBAS, SqeeSAR, etc., are successfully

employed to measure minor deformations caused by natural events or human intervention [12-14]. The achievements in dam monitoring using SAR imagery show that MT-InSAR methods have the potential to support the development of new and more effective means to monitor dam health. The free availability of high-quality SAR data with the launches of Sentinel-1A (April 2014) and Sentinel-1B (April 2016) that use C-band SAR data (frequency: 5.405GHz) helped researchers develop new tools and methods in dam surveys. Sentinel-1 Single Look Complex (SLC) images are characterized by a high spatial resolution of 5×20m and high temporal resolution. The constellation of the two satellites involved a repetition time of 6 days (Sentinel-1 B was lost after December 2021) and the resulting data was provided in near real-time [15-16].

This study used C-band radar data from the European satellites Sentinel-1A/B to derive mean Line of Site (LoS) velocity maps in the Kramis dam (Algeria), a structure oriented in the WNW-ESE direction, and its surrounding area. The Sentinel-1 satellites' four distinct tracks were used to construct the times series displacements and velocities from July 2019 to June 2021 using the Parallel SBAS (P-SBAS) method available at the Geohazards service [17–19]. The trend and seasonal components were extracted from the time series, and then the 3D displacement maps were produced.

II. METHODOLOGY

A. Processing Methodology

This study used the Parallel Small Baseline Subset (P-SBAS) approach [17–18], a multi-temporal advanced SAR interferometry method to determine Kramis dam's surface displacements, as shown in Figure 1. Using the P-SBAS service, the multi-temporal processing was carried out on the Geohazards Exploitation Platform (GEP) [19]. The user's input is only required at the beginning of the process to select the dataset, while the temporal coherence, the Digital Elevation Model (DEM), the area to process, and the entire processing are automated. The interferometric couples were chosen using the default parameters of 400m for the perpendicular baseline and 300 days for temporal separation. Eventually, a parallelized chain was used to handle the SBAS data, allowing for time optimization.

Fig. 1. The proposed workflow.

The primary aspects of the P-SBAS processing chain for Sentinel-1, presented in [19], are comparable to those of the original P-SBAS method presented in [17]. This method was developed to efficiently use distributed computing infrastructures to process multi-temporal stripmap SAR datasets. Application cases and capacity analysis of the original P-SBAS can be found in [20]. When it comes to the parallelization method, the key changes in this Sentinel-1 P-SBAS processing chain focus on achieving a higher level of granularity than the stripmap mode technique [17], which results from burst partitioning that distinguishes the S-1 IW data structure. This method allows to gather several independent bursts for each SAR scene that can be handled and processed separately, from the ingestion of input data up to the generation of DInSAR interferograms, thereby promoting the inherent parallelization of the S-1 IW interferometric processing on a burst basis.

B. Time Series Analysis

A time series is a chronological sequence of observations on a variable, in this case, the displacement in time of a Persistent Scatterer (PS). Time series analysis aims to characterize time series and develop a mathematical model that describes the evolution of the variable over time [21-22]. Moreover, different deformation patterns might cross over. A time series for dam monitoring often includes a seasonal component and a linear trend. The dam body faces subsidence as a result of the dead load of the reservoir's water as well as the settlement of the materials employed in its construction. The reservoir's water level may fluctuate over time as a result of variations in the water entering the reservoir and leaving it for irrigation, freshwater usage, or power generation. A cyclical change between subsidence and uplift could be brought on by the varying water levels [23]. Consequently, different deformation models should be considered and evaluated to determine the best-fitting model. It is worth mentioning that similar approaches were proposed in [24-26], the most relevant being linear, quadratic, and piecewise linear models for the approximation of the time series trend component. A sinusoidal [27] or a statistical model, such as the ARIMA model [28], can be used to approximate the seasonal component of the time series.

The final step in the dam deformation analysis is related to the estimation of the 3-D displacement time series based on the results of the different tracks (ascending and descending). The whole displacement vector $U = (d_e, d_n, d_u)$, where d_e, d_n, d_u are the East-West, North-South, and Up-Down directions respectively, is related to the LoS displacement by $d = \hat{P}U$, therefore $\hat{P}$ is the unit vector defined as [29]:

$$\hat{P} = [-cos\alpha_h sin\theta_{inc} \quad sin\alpha_h sin\theta_{inc} \quad cos\theta_{inc}] \quad (1)$$

where α_h and θ_{inc} are the heading and the incidence angles, respectively. The corresponding LoS displacement for each track can then be written, according to (1), as:

$$d = d_u \cos(\theta_{inc}) - \sin(\theta_{inc})[d_n \cos(\alpha_h) + d_e \sin(\alpha_h)]$$

and finally, the 3D displacement vector can be retrieved by:

$$U = -\left[\hat{P}^T \Sigma_d^{-1} \hat{P}\right]^{-1} \hat{P}^T \Sigma_d^{-1} d \quad (2)$$

III. STUDY AREA

This study investigated the deformation of the Kramis dam located in Mostaganem, Algeria, situated at the South-East of the capital of the municipality of Achaacha (Wilaya of Mostaganem) and North-East of the capital of the municipality of Nekmaria, approximately 80Km east of the town of Mostaganem and 14Km from the Mediterranean Sea, and positioned at 0°40'30"E and 36°13'00"N, as shown in Figure 2.

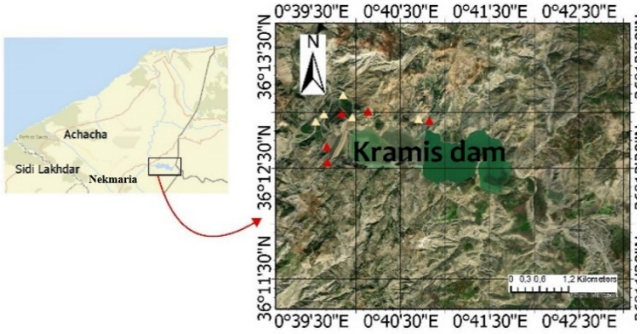

Fig. 2. The geographical location of the Kramis dam. The red triangles represent ascending CRs and the yellow descending CRs.

The Kramis dam was intended to irrigate the Achaacha Municipality perimeter with an area of 4,300ha for an affected volume of 10 million m^3 and strengthen the Dahra area network (Sidi Lakhdar, Nekmaria, Ouled Boughalem, and Achaacha) with a total population of 11,546 inhabitants (2003), with an affected volume of 5.3 million m^3. Geodetic monitoring of the Kramis dam started in May 2019, with the installation of markers for the GNSS survey and 10 Corner Reflectors (5 CRs in each Sentinel-1 acquisition direction) around the dike to be used for the calibration of the DInSAR results, since GNSS also observed all CRs [30].

IV. DATASETS

This study used C-band radar data (~5,6cm wavelength) from the European satellite Sentinel-1 to analyze the Kramis dam deformation. Forty-eight ascending and forty-eight descending Sentinel-1A/B TOPSAR images were used, covering the Kramis dam area with a one-month revisit period, from July 2019 (one month after full CRs installation (May-June 2019) [30]) to June 2021 for both acquisitions (ascending and descending), see Figure 3.

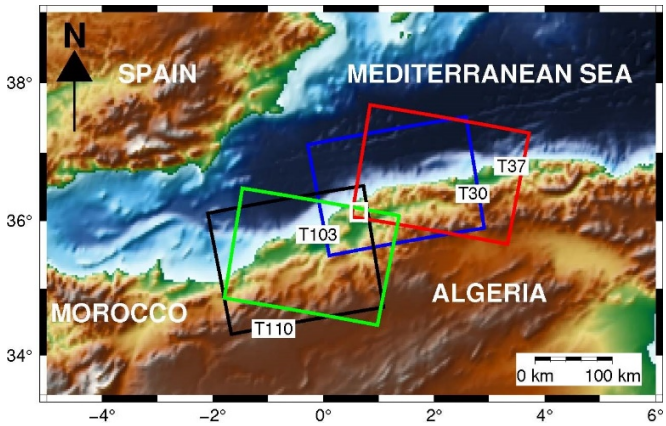

Fig. 3. Sentinel-1 paths used in this study. The white square located in the intersection of the four tracks represents the study area.

A three-arc-second (90m) Shuttle Radar Topography Mission (SRTM) DEM provided by the National Aeronautics and Space Administration (NASA) was used to remove the topographic phase component [31]. Precise Orbit Determination (POD) data provided by the European Space Agency were applied for orbital refinement and phase reflattening. A total of 24 images per track was used, one for each month over two years. The LoS displacements were referenced to the first acquisition date. The observation pillar G02 was taken as a reference for the observation of GNSS and SBAS, which was considered stable in this period, as shown in Figure 4. The displacement time series generated from the four tracks covered an area of 250×250Km^2 for each of them, and the surveyed area was about 9×12Km^2. A geographic subset was made on the four LoS time series displacements to cover the object area only for analysis.

V. RESULTS AND DISCUSSION

The Kramis Dam was imaged in ascending and descending modes and with different incidence angles. Paths 30 and 37 were acquired with incidence angles of 35° and 45°, respectively; the same was valid for tracks 103 and 110, which were tacking acquisitions in this area with incidence angles of 37°and 54°, respectively. These differences led to different numbers of distributed scatterers in the results, even when the acquisitions were made during similar month periods. Figure 4 shows the mean LoS velocity maps derived from the P-SBAS processing of the four tracks. According to this figure, a subsidence pattern can be observed on the left bank of the dam dike, as this area suffers from continuous subsidence starting from the left bank of the upstream and regularly occurring landslides [32].

The P-SBAS method indicates that the dam dike analyzed was subjected to deformation on the order of -2 to 4mm/yr in the LoS direction, with a low standard deviation of about 1mm/yr for the four tracks. The bulk of PS points that display deforming motion are also found within the top portion of the dam body, with a maximum velocity reaching 4.25mm/yr. In the case of Sentinel-1, which acquires images in a right-looking orientation, the ascending and descending geometries from the same period are the sole measurements to compute the entire movement vector. The East, North, and Up components of track 30's unit vector (-0.5467327, -0.1007871, 0.8312191), respectively, show that the sensitivity of the LoS to the North-South direction is less than 10%, making it difficult to detect movements in that direction. The same comment about the unit vector can be addressed for the remaining paths as to the contribution of the North-South direction to the unit vector, as it is less significant than the other components.

The displacement time series in Figure 4 shows how the four CRs moved over two years following their installation in June 2019. Three CRs (numbers 1, 8, 9) were destroyed and number 10 was moved from its place. Monitoring these CRs was not possible after January 2020. Most of the CRs placed around the dam body exhibited subsidence at varying intensities. As expected, CR6, which was located in a region plagued by ongoing landslides, had the highest cumulative displacement over the research period, at 20mm. However, CR5 had a 3 mm/yr uplift rate. It is worth mentioning that the velocity precision on the dike was around 1mm/yr and varied from 1 to 2.5mm/yr for the dam area.

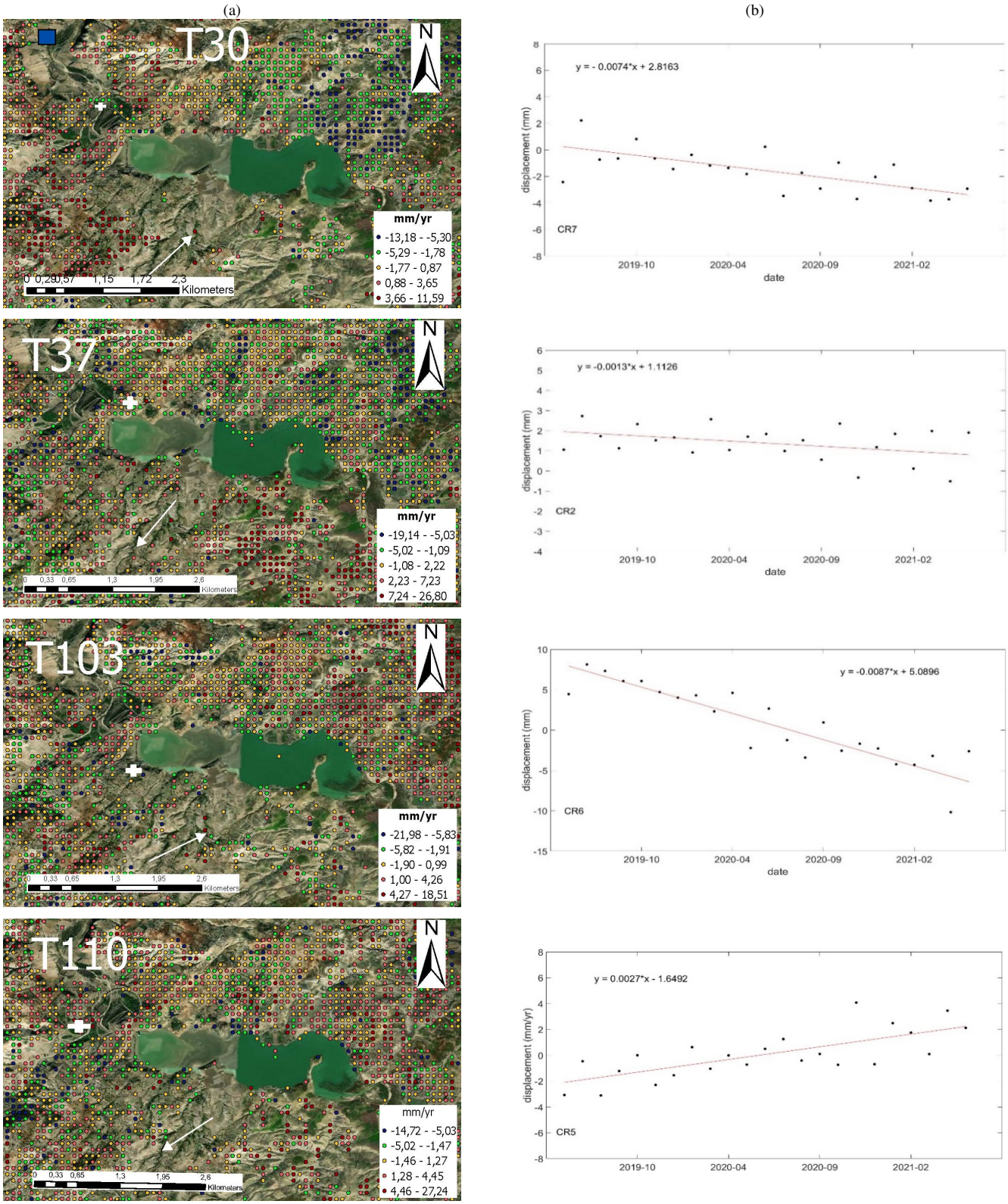

Fig. 4. Column (a): From top to bottom, mean LoS velocity for Sentinel-1 processed tracks 30, 37, 103, and 110, respectively. The white arrow corresponds to the LoS direction and the blue line in the first map stands for the reference point. Column (b): Examples of the time series displacements from the corresponding corner reflectors, where the red line corresponds to the best-fitting line, the formula of each regression line is reported in the plots.

The seasonal term from LoS observations must be extracted in an analytical step before the computation of the 3-dimensional displacement. This study used the following steps:

- Detrend the time series using a linear model.
- Subtraction of the seasonal term estimated by the application of a moving average.
- Add back the trend to the corrected time series.

TABLE I. COMPARISON BETWEEN DISPLACEMENTS OBTAINED FROM P-SBAS AND GPS PROJECTED IN LOS DIRECTION

Corner reflector	GPS-LoS (mm)	InSAR-LoS (mm)	Difference (mm)
CR2	-0.9942	-0.5239	-0.4703
CR5	6.3542	5.1927	1.1615
CR6	-24.9600	-22.5237	-2.4363
CR7	-10.98	-11.38	0.4

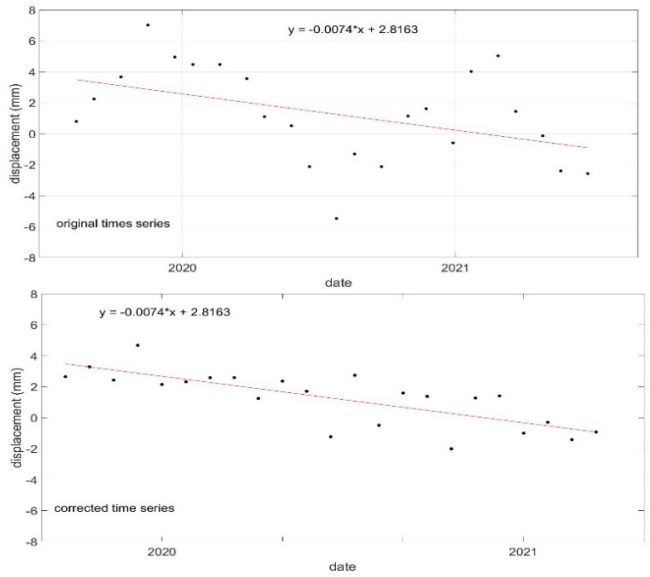

Fig. 5. Example of original and corrected time series.

Figure 5 shows the displacement of a distributed scatterer placed upstream of the Kramis dam dike, illustrating the rectification of the displacement time series from the seasonal term, where the original time series exhibits the seasonal term and subsidence. The data were detrended using a linear model and then a moving average with a sliding window of length 3 was used to estimate the seasonal component. The seasonal pattern was removed to show the displacement component. After that, the linear trend was reintroduced to get the results. Once this correction is used, it is possible to generate the 3-D displacement using (2). Figure 6 shows the results, indicating a visible settlement of the dike in the Up-Down displacement.

VI. CONCLUSION

This paper described the potential of C-band SAR Sentinel-1 data to monitor dam deformation using the advanced MT-InSAR P-SBAS method. The results showed that the Kramis dam dike had a linear deformation trend that reached 4mm/yr, except for the left bank which was subsiding at a rate of -2mm/yr. The CRs installed in the vicinity of the dike showed a subsidence movement with a rate of -3mm/yr, while CR5, located 300m from the dike, presented an uplift pattern. Time series analysis is a key step in understanding dam deformation. For this purpose, the seasonal component was estimated using a moving average with a sliding window of length 3 and removed to clean off the LoS displacements, specifically when the final objective is the estimation of the 3D displacement. The estimated Up-Down displacement showed an expected settlement for this kind of dam. The results obtained from the P-SBAS processing on different Sentinel-1 tracks showed the benefit of using cloud services for dam monitoring in Algeria, as it is possible to install a survey service for the entire dam network of the country for use by non-experts.

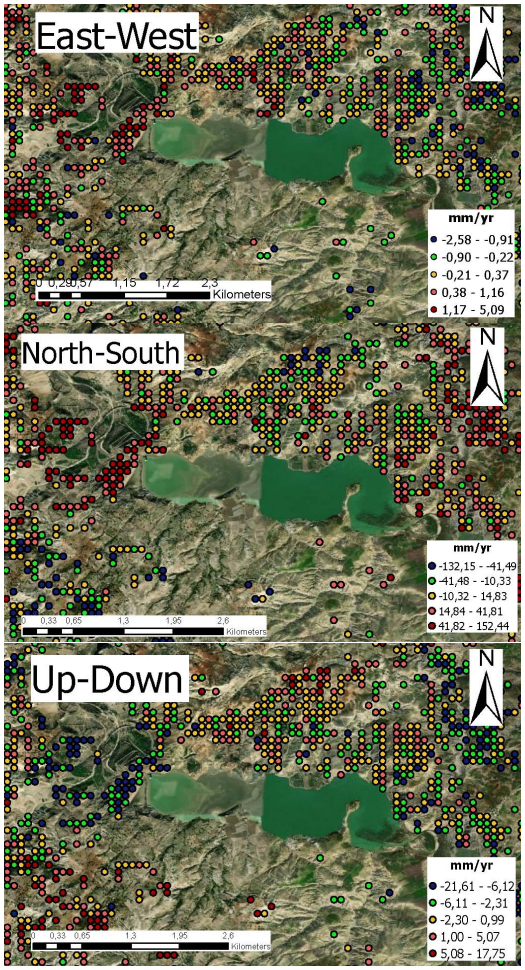

Fig. 6. 3D displacement velocities.

REFERENCES

[1] A. Benaissa, Z. Aloui, M. S. Ghembaza, H. Trouzine, and Y. Sebaibi, "Physical and Mechanical Properties of the Muds of the Fergoug Dam," *Engineering, Technology & Applied Science Research*, vol. 4, no. 4, pp. 673–676, Aug. 2014, https://doi.org/10.48084/etasr.451.

[2] Z. Zou *et al.*, "A model for interpreting the deformation mechanism of reservoir landslides in the Three Gorges Reservoir area, China," *Natural*

Hazards and Earth System Sciences, vol. 21, no. 2, pp. 517–532, Feb. 2021, https://doi.org/10.5194/nhess-21-517-2021.

[3] A. H. Bhutto, S. Zardari, G. S. Bhurgri, M. A. Zardari, R. Bhanbhro, and B. A. Memon, "Post Construction and Long Term Settlement of an Embankment Dam Computed with Two Constitutive Models," *Engineering, Technology & Applied Science Research*, vol. 9, no. 5, pp. 4750–4754, Oct. 2019, https://doi.org/10.48084/etasr.3070.

[4] A. Liaghat, A. Adib, and H. R. Gafouri, "Evaluating the Effects of Dam Construction on the Morphological Changes of Downstream Meandering Rivers (Case Study: Karkheh River)," *Engineering, Technology & Applied Science Research*, vol. 7, no. 2, pp. 1515–1522, Apr. 2017, https://doi.org/10.48084/etasr.969.

[5] A. H. Bhutto *et al.*, "Mohr-Coulomb and Hardening Soil Model Comparison of the Settlement of an Embankment Dam," *Engineering, Technology & Applied Science Research*, vol. 9, no. 5, pp. 4654–4658, Oct. 2019, https://doi.org/10.48084/etasr.3034.

[6] A. H. Bhutto *et al.*, "Parametric Analysis of an Embankment Dam's Stability," *Engineering, Technology & Applied Science Research*, vol. 9, no. 6, pp. 5016–5020, Dec. 2019, https://doi.org/10.48084/etasr.3180.

[7] S. L. Ullo *et al.*, "Application of DInSAR Technique to High Coherence Sentinel-1 Images for Dam Monitoring and Result Validation Through In Situ Measurements," *IEEE Journal of Selected Topics in Applied Earth Observations and Remote Sensing*, vol. 12, no. 3, pp. 875–890, Mar. 2019, https://doi.org/10.1109/JSTARS.2019.2896989.

[8] R. Blom, E. Fielding, A. Gabriel, and R. Goldstein, "Radar Interferometry for Monitoring of Oil Fields and Dams: Lost Hills, California and Aswan, Egypt." Root, Oct. 25, 1999, [Online]. Available: https://dataverse.jpl.nasa.gov/dataset.xhtml?persistentId=hdl:2014/17775 .

[9] D. Tarchi, H. Rudolf, G. Luzi, L. Chiarantini, P. Coppo, and A. J. Sieber, "SAR interferometry for structural changes detection: a demonstration test on a dam," in *IEEE 1999 International Geoscience and Remote Sensing Symposium. IGARSS'99 (Cat. No.99CH36293)*, Hamburg, Germany, Jun. 1999, vol. 3, pp. 1522–1524 vol.3, https://doi.org/10.1109/IGARSS.1999.772006.

[10] T. Wang, D. Perissin, F. Rocca, and M.-S. Liao, "Three Gorges Dam stability monitoring with time-series InSAR image analysis," *Science China Earth Sciences*, vol. 54, no. 5, pp. 720–732, May 2011, https://doi.org/10.1007/s11430-010-4101-1.

[11] J. Chen, Y. Zhou, G. Chen, and M. Hao, "Decades of Ground Deformation in the Weihe Graben, Shaanxi Province, China, in Response to Various Land Processes, Observed by Radar Interferometry and Levelling," *Remote Sensing*, vol. 13, no. 12, Jan. 2021, Art. no. 2374, https://doi.org/10.3390/rs13122374.

[12] M. Schlögl, B. Widhalm, and M. Avian, "Comprehensive time-series analysis of bridge deformation using differential satellite radar interferometry based on Sentinel-1," *ISPRS Journal of Photogrammetry and Remote Sensing*, vol. 172, pp. 132–146, Feb. 2021, https://doi.org/10.1016/j.isprsjprs.2020.12.001.

[13] F. Qu *et al.*, "Mapping the Recent Vertical Crustal Deformation of the Weihe Basin (China) Using Sentinel-1 and ALOS-2 ScanSAR Imagery," *Remote Sensing*, vol. 14, no. 13, Jan. 2022, Art. no. 3182, https://doi.org/10.3390/rs14133182.

[14] A. Hooper, "A multi-temporal InSAR method incorporating both persistent scatterer and small baseline approaches," *Geophysical Research Letters*, vol. 35, no. 16, 2008, https://doi.org/10.1029/2008GL034654.

[15] "Sentinel-1 SAR - Technical Guide," *Sentinel Online*. https://copernicus.eu/technical-guides/sentinel-1-sar.

[16] "Sentinel-1 SAR User Guide," *Sentinel Online*. https://copernicus.eu/user-guides/sentinel-1-sar.

[17] F. Casu *et al.*, "SBAS-DInSAR Parallel Processing for Deformation Time-Series Computation," *IEEE Journal of Selected Topics in Applied Earth Observations and Remote Sensing*, vol. 7, no. 8, pp. 3285–3296, Dec. 2014, https://doi.org/10.1109/JSTARS.2014.2322671.

[18] C. De Luca *et al.*, "An On-Demand Web Tool for the Unsupervised Retrieval of Earth's Surface Deformation from SAR Data: The P-SBAS Service within the ESA G-POD Environment," *Remote Sensing*, vol. 7, no. 11, pp. 15630–15650, Nov. 2015, https://doi.org/10.3390/rs71115630.

[19] M. Manunta *et al.*, "The Parallel SBAS Approach for Sentinel-1 Interferometric Wide Swath Deformation Time-Series Generation: Algorithm Description and Products Quality Assessment," *IEEE Transactions on Geoscience and Remote Sensing*, vol. 57, no. 9, pp. 6259–6281, Sep. 2019, https://doi.org/10.1109/TGRS.2019.2904912.

[20] I. Zinno *et al.*, "Cloud Computing for Earth Surface Deformation Analysis via Spaceborne Radar Imaging: A Case Study," *IEEE Transactions on Cloud Computing*, vol. 4, no. 1, pp. 104–118, Jan. 2016, https://doi.org/10.1109/TCC.2015.2440267.

[21] K. Neusser, *Time Series Econometrics*. Springer International Publishing, 2016.

[22] D. C. Montgomery, C. L. Jennings, and M. Kulahci, *Introduction to Time Series Analysis and Forecasting*. Hoboken, NJ, USA: John Wiley & Sons, 2015.

[23] M. Evers, A. Thiele, H. Hammer, E. Cadario, K. Schulz, and S. Hinz, "Concept to Analyze the Displacement Time Series of Individual Persistent Scatterers," *ISPRS - International Archives of the Photogrammetry, Remote Sensing and Spatial Information Sciences*, vol. 43B3, pp. 147–154, Jun. 2021, https://doi.org/10.5194/isprs-archives-XLIII-B3-2021-147-2021.

[24] M. Berti, A. Corsini, S. Franceschini, and J. P. Iannacone, "Automated classification of Persistent Scatterers Interferometry time series," *Natural Hazards and Earth System Sciences*, vol. 13, no. 8, pp. 1945–1958, Aug. 2013, https://doi.org/10.5194/nhess-13-1945-2013.

[25] M. Evers, A. Kyriou, A. Thiele, H. Hammer, K. Nikolakopoulos, and K. Schulz, "How to set up a dam monitoring system with PSInSAR and GPS," in *Earth Resources and Environmental Remote Sensing/GIS Applications XI*, Sep. 2020, vol. 11534, pp. 98–114, https://doi.org/10.1117/12.2573880.

[26] S. M. Mirmazloumi *et al.*, "Classification of ground deformation using sentinel-1 persistent scatterer interferometry time series," *GIScience & Remote Sensing*, vol. 59, no. 1, pp. 374–392, Dec. 2022, https://doi.org/10.1080/15481603.2022.2030535.

[27] J. W. Bell, F. Amelung, A. Ferretti, M. Bianchi, and F. Novali, "Permanent scatterer InSAR reveals seasonal and long-term aquifer-system response to groundwater pumping and artificial recharge," *Water Resources Research*, vol. 44, no. 2, 2008, https://doi.org/10.1029/2007WR006152.

[28] X. Wang, Q. Yu, J. Ma, L. Yang, W. Liu, and J. Li, "Study and Prediction of Surface Deformation Characteristics of Different Vegetation Types in the Permafrost Zone of Linzhi, Tibet," *Remote Sensing*, vol. 14, no. 18, Jan. 2022, Art. no. 4684, https://doi.org/10.3390/rs14184684.

[29] T. J. Wright, B. E. Parsons, and Z. Lu, "Toward mapping surface deformation in three dimensions using InSAR," *Geophysical Research Letters*, vol. 31, no. 1, 2004, https://doi.org/10.1029/2003GL018827.

[30] B. Gourine, K. Hasni, "First Algerian Experiment of Manufactured Corner Reflectors for An Embankment DAM monitoring: case of kramis DAM (Mostaganem, Algeria)", presented at World Multidisciplinary Earth Sciences Symposium (WMES 2019), Prague, Czech Republic, Sep. 2019.

[31] B. Rabus, M. Eineder, A. Roth, and R. Bamler, "The shuttle radar topography mission—a new class of digital elevation models acquired by spaceborne radar," *ISPRS Journal of Photogrammetry and Remote Sensing*, vol. 57, no. 4, pp. 241–262, Feb. 2003, https://doi.org/10.1016/S0924-2716(02)00124-7.

[32] B. Gourine, K. Hasni, S. H. Allal, " Deformation monitoring of Kramis's Dam region (State of Mostaganem, Algeria) by Radar Interferometry using SBAS technique: First results", presented at Fringe 2021 – 11th International Workshop on Advances in the Science and Applications of SAR Interferometry, Amsterdam, Netherlands, Jun. 2021.